Dynamic discrimination of oriented molecules controlled with the nonresonant dynamic Stark effect induced by a single-cycle THz pulse

Yuzuru Kurosaki,[1,*] Hiroshi Akagi,[2] and Keiichi Yokoyama[2]

[1]*Quantum Beam Science Center, Tokai Research and Development Center, Japan Atomic Energy Agency, Tokai, Ibaraki 319-1195, Japan*

[2]*Quantum Beam Science Center, Kansai Photon Science Institute, Japan Atomic Energy Agency, Kizugawa, Kyoto 619-0215, Japan*

(Received 12 August 2014; published 8 October 2014)

We theoretically propose a control scheme of temporal wave-packet separation for oriented molecules, based on nonresonant dynamic Stark effect (DSE) in the dipole limit. The proposed scheme exploits the fact that diabatic coupling between the lowest two potential-energy curves (PECs) depends on diatomic internuclear distance. In the control process nonresonant DSE shifts the PECs, moves the avoided crossing position, and thus changes transition probability from one PEC to another. In the scheme linearly polarized single-cycle THz pulses are employed as control fields and are applied to the molecules oriented along the field polarization. In this paper the proposed scheme is applied to the temporal wave-packet separation of the binary mixture of alkali-halide isotopologues ^{133}CsI and ^{135}CsI. We assume that before applying the control pulse one of the isotopologues is oriented along the field polarization direction and the other is oriented along the opposite direction (isotope-dependent orientation) and then they are electronically excited from the ground-state PEC to the excited-state counterpart. Numerical wave-packet propagations under some control pulses reveal that a THz pulse yields a temporal wave-packet separation of about 2 ps between the two isotopologue photodissociations. We also consider the cases where the molecular axis is not parallel to the field polarization direction and carry out the same wave-packet calculations. It is found, as a result, that the temporal wave-packet separation is comparable with the parallel case, indicating that even when the isotope-dependent orientation right before control is not perfectly achieved, the proposed control scheme works well. This result suggests that the present separation scheme for oriented molecules is more robust against imperfect orientation than the molecular separation technique using the dependence of electronic transition probability on the field polarization direction relative to the molecular axis.

DOI: 10.1103/PhysRevA.90.043407 PACS number(s): 32.80.Qk, 33.80.Wz, 82.50.Nd

I. INTRODUCTION

The past two decades have seen remarkable progress in quantum control with ultrashort laser pulses [1–3], which has a great chance for making a breakthrough in future technology. Recently, the so-called dynamic Stark effect (DSE) with intense laser fields has been regarded as a key to control chemical reactions [4–11] since it can shift potential-energy surfaces and change the transition probability to a target. Depending on the laser frequency, DSE can be classified into resonant and nonresonant regimes. The nonresonant type might be more promising because in this regime excitations to other electronic states are suppressed, which often lead to undesirable competing pathways. It is known that there are two limiting cases in the nonresonant DSE: the Raman limit [4–7] and the dipole limit [8–11]. In the former case the interaction only follows the laser-pulse envelope, whereas in the latter it follows the instantaneous laser field. The present paper explores a control scheme based on the nonresonant DSE in the dipole limit.

Several groups [8–11] have theoretically studied the control of alkali-halide photodissociation via an avoided crossing (AC) on the basis of the nonresonant DSE in the dipole limit. Han *et al.* [8] demonstrated that a branching ratio between the ionic and the covalent pathways for the NaI molecule can be changed with the nonresonant DSE because the Stark pulse changes the energy difference between the ground and the excited potential-energy curves (PECs). Liu *et al.* [9] investigated the manipulation of the branching ratio for the NaI molecule and found that the velocity of a wave packet at the AC, which can be altered with the nonresonant DSE, is essential to the ratio. Recently, Scheit *et al.* [10,11] have presented detailed discussions on how the nonadiabatic transition at the AC can be controlled by modulating the applied laser parameters, such as pulse intensity, frequency, phase, and time difference between pump and control pulses, using the LiF molecule as an example.

We focus here on the strong dependence of diabatic coupling on the internuclear distance for diatomic alkali halides [10–13]; the coupling is very large around the potential minimum, but it rapidly decreases as internuclear distance increases. Scheit *et al.* [11] have fully investigated nonadiabatic dynamics affected by the coordinate dependence of diabatic coupling through the potential shiftings with the nonresonant DSE, and in the present paper we propose a control scheme that directly makes use of the coordinate dependence of diabatic coupling. We theoretically demonstrate the validity of the scheme by applying it to the temporal wave-packet separation of the cesium iodide isotopologues ^{133}CsI and ^{135}CsI with a single-cycle THz pulse.

The paper is organized as follows. Section II describes the diabatization procedure to obtain diabatic PECs and dipole moments (DMs) that are used in the calculation. The scheme of quantum control proposed here is presented in Sec. III. The wave-packet propagation procedure is described in Sec. IV, and the parameters of the applied THz pulses are given in Sec. V. Section VI shows computational results and discusses the validity of the control scheme. Finally, the paper is concluded with some remarks in Sec. VII.

*kurosaki.yuzuru@jaea.go.jp

II. DIABATIC PECS

Previously, we [14] calculated the PECs of CsI, originated from the ground states of the neutral and ionic asymptotes, using the multireference configuration interaction method including the spin-orbit effect with the relativistic pseudopotentials. We use those data for the lowest two adiabatic Σ^+ PECs, and we perform some additional calculations at more points of internuclear distance (R) to fill the shortage in the original data. The diabatic potentials are used in the present time-dependent wave-packet calculations; the diabatic representation is more convenient than the adiabatic counterpart for solving time-dependent Schrödinger equations for dynamics on coupled electronic states because the nuclear kinetic-energy operator is diagonal and the coupling terms are included in the off-diagonal elements of the potential matrix.

The relation between the adiabatic (superscript a) and the diabatic (superscript d) representations for two electronic states ϕ_1 and ϕ_2 is generally given by [15]

$$\begin{pmatrix} \phi_1^d \\ \phi_2^d \end{pmatrix} = \mathbf{U} \begin{pmatrix} \phi_1^a \\ \phi_2^a \end{pmatrix}, \tag{1}$$

where

$$\mathbf{U} = \begin{pmatrix} \cos\ \alpha(R) & \sin\ \alpha(R) \\ -\sin\ \alpha(R) & \cos\ \alpha(R) \end{pmatrix} \tag{2}$$

is the transformation matrix with $\alpha(R)$ being the mixing angle at R. The diabatization in the present study is performed using the transformation matrix $\mathbf{U}$ that diagonalizes the DM matrix [10–13],

$$\boldsymbol{\mu}^d = \mathbf{U}^+ \boldsymbol{\mu}^a \mathbf{U}, \tag{3}$$

where $\boldsymbol{\mu}^a$ is the DM matrix in the adiabatic representation and $\boldsymbol{\mu}^d$ is the diagonal DM matrix in the diabatic representation.

The diabatic quantities obtained based on Eqs. (1)–(3) are displayed in Fig. 1: Figure 1(a) shows the lowest two adiabatic Σ^+ PECs V_{11}^a and V_{22}^a, the corresponding two diabatic Σ^+ PECs V_{11}^d and V_{22}^d, and the diabatic coupling V_{12}^d; Fig. 1(b) depicts the two adiabatic DMs μ_{11}^a and μ_{22}^a, the adiabatic transition dipole moment (TDM) μ_{12}^a, and the corresponding two diabatic DMs μ_{11}^d and μ_{22}^d; Fig. 1(c) gives the mixing angle α for the adiabatic-diabatic transformation. As shown in Fig. 1(a), there is a slight difference between the adiabatic and the diabatic PECs when R is small but almost no difference when it is large. In the asymptotic limit the adiabatic and diabatic representations are identical, and the values of V_{11} and V_{22} are −314.807 03 and −314.853 30 a.u., respectively. It is noteworthy that the diabatic coupling V_{12}^d has the maximum around the potential minimum of V_{11}^d and it is nearly zero around the AC. This result agrees well with the previous calculations for other diatomic alkali halides: LiF [12] and NaI [13]. The diabatization described above yields the smooth diabatic DMs μ_{11}^d and μ_{22}^d and the zero diabatic TDM by definition as shown in Fig. 1(b). There is a small difference between the adiabatic and the diabatic DMs when R is small and almost no difference when it is large.

The theoretical prediction that diabatic coupling V_{12}^d has its maximum not around the AC but around the potential minimum is due to the fact that adiabatic DM matrix $\boldsymbol{\mu}^a$ is

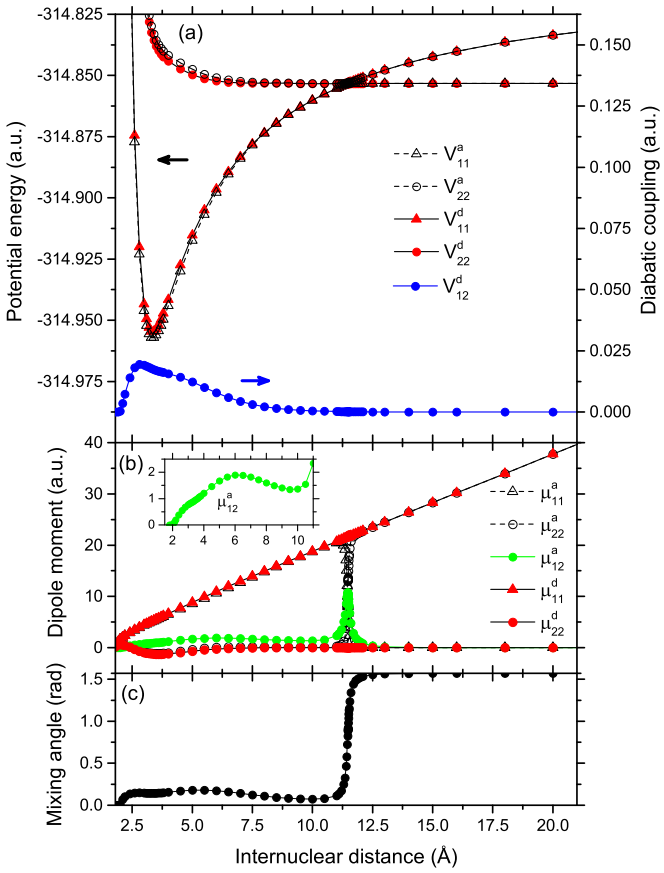

FIG. 1. (Color online) (a) The lowest two adiabatic Σ^+ PECs (V_{11}^a and V_{22}^a), the corresponding two diabatic Σ^+ PECs (V_{11}^d and V_{22}^d), and the diabatic coupling (V_{12}^d); (b) the two adiabatic DMs μ_{11}^a and μ_{22}^a, the adiabatic TDM μ_{12}^a, and the corresponding two diabatic DMs μ_{11}^d and μ_{22}^d; (c) mixing angle for the adiabatic-diabatic transformation.

nondiagonal at $R < 10$ Å as shown in Fig. 1(b); the inset shows that μ_{12}^a has a minimum of about 1.3 a.u. at around $R = 10$ Å, has a maximum of about 1.9 a.u. at around $R = 6$ Å, and decreases monotonically when $R < 6$ Å, finally reaching zero at $R = 1.8$ Å. Diagonalizing $\boldsymbol{\mu}^a$ to obtain $\boldsymbol{\mu}^d$ based on Eq. (3) results in the mixing angle plotted in Fig. 1(c), showing that it has a maximum of about 0.2 at around $R = 5$ Å. From Eqs. (1) and (2) the relation between diabatic coupling V_{12}^d and the adiabatic potentials V_{11}^a and V_{22}^a is given by

$$V_{12}^d = V_{21}^d = (1/2)\left(V_{22}^a - V_{11}^a\right) \sin\ 2\alpha, \tag{4}$$

and, as a result, V_{12}^d has its maximum around the potential minimum as shown in Fig. 1(a).

III. PROPOSED CONTROL SCHEME

The control scheme proposed here directly makes use of the coordinate dependence of V_{12}^d given in Fig. 1(a). In the control scenario based on nonresonant DSE an appropriate laser pulse causes upward or downward potential shifting, displacing left or right the potential crossing as a result, and thus changing the transition probability at the crossing between diabatic PECs. The potential shiftings can be used to

temporally separate the wave packets of oriented molecules; as an example of the applications, the binary mixture of diatomic alkali-halide isotopologues ^{133}CsI and ^{135}CsI is considered in the present study. The control scheme of the temporal wave-packet separation of the isotopologues is described in a few steps as follows: (1) One of the isotopologues is oriented along one direction, and the other is oriented along the opposite direction (isotope-dependent orientation); (2) thus oriented isotopologues are electronically excited from V_{11}^d to V_{22}^d with a pump pulse; (3) a linearly polarized control pulse (single-cycle THz pulse) is applied so that the field polarization vector is parallel to the oriented molecular axes.

In step 1 a high degree of isotope-dependent molecular orientation needs to be achieved. Molecular alignment and orientation have been a topic of great interest in the recent quantum-control study. Note that a molecule is said to be aligned when its axis is parallel to a definite direction and to be oriented when the head-versus-tail order is also controlled in addition to alignment. It has been reported so far that molecular orientation was experimentally achieved with: (a) the combinations of an electrostatic field and an intense nonresonant laser field [16–19], (b) two-color laser fields [20,21], and (c) an intense THz field [22]; in any of these techniques molecular orientation is observed at every rotational period. Because of the difference in rotational period between ^{133}CsI and ^{135}CsI, isotope-dependent orientation can be achieved after some delay time from the irradiation of an appropriate laser pulse, which might be explained using a simple example as follows. First, the coherent superposition state of the $J = 0$ and $J = 1$ rotational states is created for each isotopologue. This is the simplest oriented state that can be realized using a THz pulse. Then, the isotope-dependent orientation is achieved after the delay time of about 48.78 ns, corresponding to the 69th rotational period of ^{133}CsI and the 68.5th period of ^{135}CsI, estimated from the rotational periods of the isotopologues: 706.91 and 712.07 ps calculated using the observed rotational constant of ^{133}CsI [23] and the atomic masses [24]. The effect of collisions between the molecules can be neglected in this delay time unless the experiment is performed under high-pressure conditions. Recently, using the homonuclear diatomic isotopologues $^{14}N_2$ and $^{15}N_2$, we [25] have experimentally created the situation that one isotopologue is aligned to a direction and the other is laid in the plane perpendicular to the direction based on field-free alignment after a short laser-pulse irradiation, followed by isotope-selective ionization with another laser pulse.

We assume that the isotope-dependent orientation of the isotopologues is achieved in step 1 and then the electronic excitation from V_{11}^d to V_{22}^d concurrent with the orientation is completed in step 2. In the present paper we thus concentrate our discussion on step 3 where the wave packets for the isotopologues are propagated on the two diabatic PECs under a control THz pulse.

Step 3 includes the essence of the control scheme where the DSE plays a key role. For simplicity, the initial condition for the time-dependent wave-packet propagation is set to be the vibrational ground-state wave function for V_{11}^d just placed on V_{22}^d. We also assume the rotational motion is frozen during the wave-packet propagation; this might be justified because the rotational period of the CsI molecule, which is more than

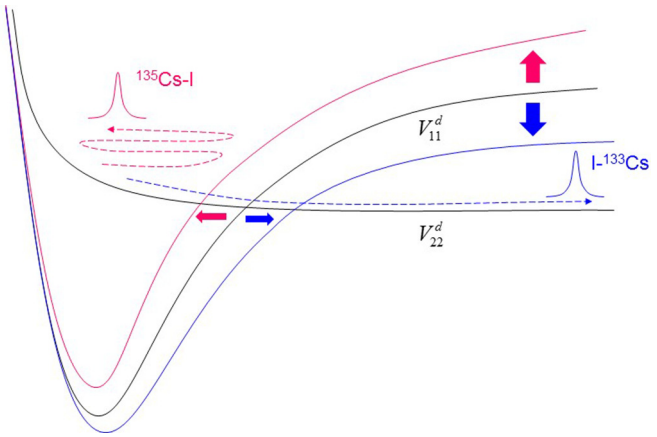

FIG. 2. (Color online) Sketch of the proposed control scheme for temporal isotope-selective separation that directly uses the dependence of diabatic coupling on internuclear distance; the DSE-based potential shifting moves the AC position and changes transition probability from one state to another.

700 ps when considering the $J = 0$ and $J = 1$ rotational states, as discussed above, is much longer than the pulse durations used in this paper. As illustrated in Fig. 2, when a control THz pulse is applied to the isotopologues that achieved the isotope-dependent orientation in step 1, the DSE creates the situation that diabatic PEC V_{11}^d for one isotopologue shifts upward (vertical red arrow) whereas that for the other shifts downward (vertical blue arrow) and, as a result, the AC for one isotopologue moves left (horizontal red arrow) and that for the other moves right (horizontal blue arrow). Since the diabatic coupling between the two diabatic PECs strongly depends on R as shown in Fig. 1(a) with its maximum being around the potential minimum of V_{11}^d, it is expected that the wave packet for one isotopologue is confined in the upper adiabatic potential (wave packet in red) because of the large diabatic coupling, whereas that for the other goes to dissociation (wave packet in blue) because of the small diabatic coupling or no crossing. Since the control field temporally oscillates, the confined wave packet will eventually go to dissociation, but the wave packets for the two isotopologues are thus temporally separated, and the confined wave packet could be deexcited to the ground-state PEC again with another laser pulse to complete an isotope-separation process. Theoretically, perfect deexcitation of the confined wave packet to the ground-state PEC might be possible using the control field obtained with optimal control theory [26]; experimentally, however, theoretically predicted control is often impossible because of great difficulty in creating the calculated control fields despite the state-of-the-art pulse-shaping technology. We nevertheless emphasize that the confined wave packet can be deexcited at least partially and some degree of isotope selectivity is obtained with the available laser techniques.

IV. WAVE-PACKET PROPAGATION

The time-dependent wave-packet propagation technique is used to investigate control dynamics on the two diabatic PECs. The time-dependent Schrödinger equation on the two PECs

can be written in a matrix form,

$$i\frac{\partial}{\partial t}\boldsymbol{\psi} = \mathbf{H}\boldsymbol{\psi}, \tag{5}$$

where

$$\boldsymbol{\psi} = \begin{pmatrix}\psi_1(t)\\ \psi_2(t)\end{pmatrix}, \tag{6}$$

with $\psi_1(t)$ and $\psi_2(t)$ being the projections of the system wave packet on diabatic PECs V_{11}^d and V_{22}^d, respectively. The molecular rotational motion is frozen in the present calculations, and the Hamiltonian matrix is represented as

$$\mathbf{H} = \mathbf{T} + \mathbf{V} = -\frac{1}{2m}\mathbf{I}\frac{d^2}{dR^2} + \mathbf{V}, \tag{7}$$

where m is the molecular reduced mass, $\mathbf{I}$ is the 2×2 unit matrix, and $\mathbf{V}$ is the potential-energy matrix given by

$$\mathbf{V} = \begin{pmatrix}V_{11} & V_{12}\\ V_{21} & V_{22}\end{pmatrix} = \begin{pmatrix}V_{11}^d - \mu_{11}^d\varepsilon(t) & V_{12}^d\\ V_{21}^d & V_{22}^d - \mu_{22}^d\varepsilon(t)\end{pmatrix}. \tag{8}$$

In Eq. (8) $\varepsilon(t)$ is the electric field applied to the isotopic binary mixture. The off-diagonal elements of $\mathbf{V}$ are responsible for the transitions between the two diabatic PECs due to the diabatic couplings V_{12}^d and V_{21}^d. Note that the dipole coupling is zero by definition. Equation (5) is numerically solved using the split-operator method [27,28],

$$\boldsymbol{\psi}(t+\Delta t) = \exp(-i\mathbf{V}\,\Delta t/2)\exp(-i\mathbf{T}\,\Delta t) \times \exp(-i\mathbf{V}\,\Delta t/2)\,\boldsymbol{\psi}(t) + O(\Delta t^3). \tag{9}$$

Equation (9) is numerically integrated based on the fast-Fourier-transform algorithm that efficiently transforms the wave-function representation between the momentum and the coordinate spaces. Two total times for the numerical integration, 82 682 a.u. (2 ps) and 165 364 a.u. (4 ps), are considered (see Sec. V), and the numbers of the time steps are 4096 and 8192, respectively, i.e., the time step is 20.2 a.u. As for the exponential of the potential-energy matrix, we employ the procedures using the diabatic potential energies directly, without diagonalizing the matrix [29,30].

The initial condition ψ_0 for Eq. (2) is the vibrational ground-state wave function ϕ_1^1 for V_{11}^d just placed on V_{22}^d, i.e., $\psi_0 = (0,\phi_1^1)^{\mathrm{T}}$. Wave function ϕ_1^1 is obtained using the Fourier-grid Hamiltonian method [31] with 4096 evenly spaced grid points at an internuclear distance from 1.8 to 25 Å.

A damping function [32],

$$f(s_i) = \sin\left[\frac{\pi}{2}\frac{(s_{\mathrm{mask}} + \Delta s_{\mathrm{mask}} - s_i)}{\Delta s_{\mathrm{mask}}}\right], \quad s_i \geqslant s_{\mathrm{mask}} \tag{10}$$

is placed at the grid edge to eliminate the reflection of the wave packet at the boundary, where s_{mask} is the point at which the damping function is initiated and $\Delta s_{\mathrm{mask}} = s_{\mathrm{max}} - s_{\mathrm{mask}}$ is the region where the damping function decays from 1 to 0, with s_{max} being the maximum point of the grid. The damping function is operated only over the last ten grid points from the edge s_{max}.

V. APPLIED ELECTRIC FIELDS

We use linearly polarized single-cycle THz pulses as a control field, which have the form

$$\varepsilon(t) = Es(t)\sin(2\pi t/T), \tag{11}$$

where E is the peak amplitude, T is the total time (i.e., pulse duration), and $s(t)$ is the shape function given by

$$s(t) = \sin^2(\pi t/T). \tag{12}$$

We found in a preliminary calculation that it took about 0.5 ps for the wave packet to reach the AC region from the starting point. We choose two total times according to the wave-packet motion: $T = 82\,682$ a.u. (2 ps) and 165 364 a.u. (4 ps), corresponding to 0.5 and 0.25 THz frequencies, respectively. Four peak amplitudes are chosen: $E = 1.0\times10^{-3}$, 2.5×10^{-3}, 5.0×10^{-3}, and 1.0×10^{-2} a.u. We thus consider eight combinations of E and T and discuss the control mechanism of temporal wave-packet separation. First, the cases where the field polarization is parallel to the molecular axis (parallel cases) are investigated; those where the polarization direction and the molecule axis are not parallel (nonparallel cases) are then calculated in order to know how successful the control of temporal photodissociation is in a situation where molecular orientation is not perfect. Nonparallel cases are investigated only for the combination of E and T giving the best control revealed in the parallel cases. The angles between the polarization direction and the molecular axis are set at 10°, 20°, and 30°.

VI. RESULTS AND DISCUSSION

A. Photodissociation probability

Photodissociation probability in channel i (P_i) can be defined as the temporal accumulation of the probability flux (J_i) (i.e., cumulative flux) that is evaluated at an appropriate internuclear distance,

$$P_i = \int_0^\infty J_i(t)dt. \tag{13}$$

Using the reduced mass m and the wave-packet component on diabatic PEC V_{ii}^d, $\psi_i(R,t)$, the probability flux J_i evaluated at $R = R_f$ is expressed by

$$J_i(t) = \frac{1}{m}\mathrm{Im}\left[\psi_i^*(R,t)\frac{\partial\psi_i(R,t)}{\partial R}\right]_{R=R_f}, \tag{14}$$

where Im denotes the imaginary part. The value of R_f is chosen such that the wave packet already has the asymptotic shape at R_f but is still unaffected by an absorbing potential placed at the grid edge. Here we choose $R_f = 35$ a.u. (18.5 Å).

Figure 3 shows the cumulative fluxes at $R_f = 35$ a.u. for two channels (V_{11}^d and V_{22}^d) of ^{133}CsI and ^{135}CsI, obtained using a single-cycle THz pulse with the eight combinations of the total pulse duration and peak amplitude [Figs. 3(a)–3(h)]. In the lower panels of each figure are displayed the applied THz fields. Figures 3(a)–3(d) are for $T = 82\,682$ a.u. (2 ps), and Figs. 3(e)–3(h) are for $T = 165\,364$ a.u. (4 ps).

When $T = 82\,682$ a.u. (2 ps) and $E = 1.0\times10^{-3}$ a.u. [Fig. 3(a)], the V_{22}^d cumulative flux for ^{133}CsI rapidly increases around $t = 50\,000$ a.u. to nearly 1 and at the same time that

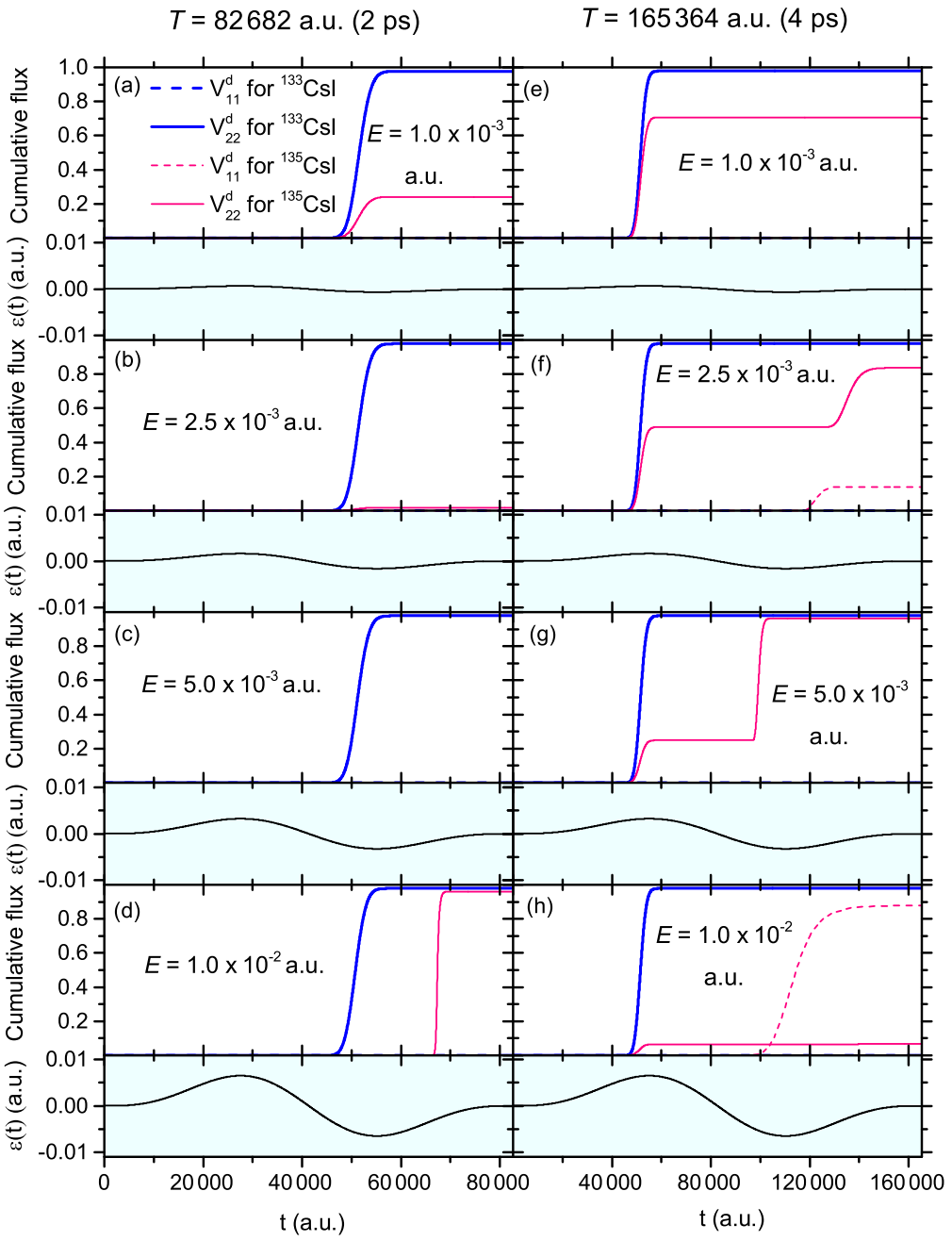

FIG. 3. (Color online) The cumulative flux at $R_f = 35$ a.u. for two channels (V_{11}^d and V_{22}^d) of ^{133}CsI and ^{135}CsI, obtained using a single-cycle THz pulse with the eight combinations of the total pulse duration and peak amplitude. Applied THz fields are displayed in the lower panels of each figure.

for ^{135}CsI increases to about 0.25. This indicates that the wave packet for ^{133}CsI initially placed on V_{22}^d goes diabatically through the AC almost totally due to the downward shifting of V_{11}^d, whereas that for ^{135}CsI mostly moves adiabatically onto V_{11}^d due to the upward shifting of V_{11}^d but a part of it goes diabatically through the AC. As shown in Fig. 3(b), increasing E to 2.5×10^{-3} a.u. does not affect the V_{22}^d cumulative flux for ^{133}CsI but reduces that for ^{135}CsI, indicating that the wave packet for ^{135}CsI goes almost adiabatically through the AC and increasing E further to 5.0×10^{-3} a.u. [Fig. 3(c)] reduces the V_{22}^d flux to almost zero. Note that the wave packet for ^{135}CsI will eventually go to dissociation after the pulse is turned off, but in the case shown in Fig. 3(c) the temporal wave-packet separation between the ^{133}CsI and the ^{135}CsI dissociation is at least about 0.8 ps, showing the temporal separation is completed. It is of interest to note that when $E = 1.0\times10^{-2}$ a.u. [Fig. 3(d)], the V_{22}^d cumulative flux for ^{135}CsI suddenly picks up around $t = 67\,000$ a.u. This might be explained as follows. A large upward shifting of V_{11}^d in the first half of the pulse uplifts the wave packet for ^{135}CsI confined in the upper adiabatic potential well, giving the potential energy to the wave packet, and in the last half of the pulse it moves toward dissociation with additional kinetic energy transformed from the gained potential energy. As a result, the V_{22}^d flux for

^{135}CsI, originated from the wave-packet portion first confined in the upper adiabatic potential well, runs faster than that in the cases with $E = 1.0\times10^{-3}$ and 2.5×10^{-3} a.u. shown in Figs. 3(a) and 3(b).

Figures 3(e)–3(h) show the results for half the frequency (0.25 THz). The cumulative fluxes shown in Fig. 3(e) exhibit the same behavior as those in Fig. 3(a) except that the V_{22}^d cumulative flux for ^{135}CsI reaches 0.7 in a total time of 4 ps, indicating that more of the portion of the wave packet goes diabatically through the AC in this case. When $E = 2.5\times10^{-3}$ a.u. [Fig. 3(f)], the V_{22}^d flux for ^{135}CsI shows a steplike behavior. The second step beginning around $t =$ 130 000 a.u. takes place because when the portion of the wave packet, first confined in the upper adiabatic potential well, goes through the AC again, it further splits into two portions because of small diabatic coupling and one goes diabatically onto V_{22}^d; the other goes adiabatically onto V_{11}^d and its flux appears from $t =$ 120 000 a.u. as shown by the red broken line. The wave packet on V_{11}^d will dissociate eventually because it is a fraction of the larger wave-packet portion that obtains some potential energy on V_{11}^d shifted upward in the first half of the pulse, and hence it has enough energy to reach the asymptotic region on V_{11}^d at the end of the pulse or after the pulse is turned off. When $E = 5.0\times10^{-3}$ a.u. [Fig. 3(g)], the second step of the V_{22}^d cumulative flux for ^{135}CsI occurs earlier than that shown in Fig. 3(f) and there is no V_{11}^d flux. This is because the confined wave packet obtains larger potential energy due to the upward shifting of V_{11}^d and goes through the AC faster, resulting predominantly in the diabatic passage to V_{22}^d with almost no adiabatic transfer onto V_{11}^d. As shown in Fig. 3(h), increasing E to 1.0×10^{-2} a.u. changes noticeably the photodissociation mechanism; the V_{11}^d cumulative flux for ^{135}CsI increases from $t =$ 100 000 a.u. In this case the wave packet for ^{135}CsI is mostly confined in the upper adiabatic potential well due to the large upward shifting of V_{11}^d, and when the wave packet again reaches the AC from the left, the diabatic coupling there is still large and it goes adiabatically onto V_{11}^d. In this case the wave packet on V_{11}^d will dissociate eventually, similar to the case with $E = 2.5\times10^{-3}$ a.u., Fig. 3(f).

As discussed above, the temporal wave-packet separation mechanism strongly depends on the parameters of the applied THz field. Among the cases considered here, the combination of $T =$ 82 682 a.u. (2 ps) and $E = 5.0\times10^{-3}$ a.u. [Fig. 3(c)] might be the best for the temporal wave-packet separation for ^{133}CsI and ^{135}CsI.

B. Wave-packet motion

In order to obtain a deeper understanding of the temporal wave-packet separation we track the motions of the V_{11}^d and V_{22}^d wave-packet components for the two isotopologues. Figures 4(a)–4(l) show temporal changes in the V_{11}^d and V_{22}^d wave-packet components (upper panel) along with the temporal shiftings of V_{11}^d and V_{22}^d due to the DSE (lower panel), propagated by the control THz pulse with $T =$ 82 682 a.u. (2 ps) and $E = 5.0\times10^{-3}$ a.u., which gave the best temporal wave-packet separation revealed in the previous subsection. Note that in the figure the wave packets are further propagated after the field is turned off at $t =$ 82 682 a.u. (2 ps).

At $t = 0$ a.u. [Fig. 4(a)] the V_{11}^d ground-state vibrational wave functions for ^{133}CsI and ^{135}CsI are placed on V_{22}^d and start to propagate under the control field. The wave functions for ^{133}CsI and ^{135}CsI placed on V_{22}^d propagate quite similarly right after they leave the initial position, and at $t =$ 15 033 a.u. (0.36 ps) they still share almost the same shape and position as displayed in Fig. 4(b). Since V_{11}^d for ^{135}CsI is shifting upward and that for ^{133}CsI is shifting downward as shown in the lower panel of Fig. 4(b), the V_{22}^d wave-packet components for the two isotopologues will experience different passages through the AC. And at $t =$ 30 066 a.u. (0.73 ps), the V_{22}^d wave-packet component for ^{135}CsI almost disappears, and the V_{11}^d component appears instead as shown in Fig. 4(c), indicating that when the V_{22}^d component encounters the left-shifted AC from the left for the first time, it predominantly goes onto V_{11}^d adiabatically because of the relatively large diabatic coupling at the AC. The V_{22}^d wave-packet component for ^{133}CsI is going to dissociation without encountering the AC because of a large downward shifting of V_{11}^d as shown in the lower panel of Fig. 4(c). When $t =$ 45 099 a.u. (1.09 ps), Fig. 4(d), the V_{22}^d wave-packet component for ^{133}CsI further advances to dissociation; it has already passed the AC diabatically where diabatic coupling is very small. The V_{11}^d wave-packet component for ^{135}CsI depicted in Fig. 4(c) goes down the slope of V_{11}^d to the left and encounters the AC from the right for the second time, splitting into the two V_{11}^d and V_{22}^d components, which are seen around $R = 7$ Å in Fig. 4(d); the V_{11}^d component is very oscillatory, implying that the wave packet obtains kinetic energy after sliding down the slope of V_{11}^d. When $t =$ 60 132 a.u. (1.45 ps), Fig. 4(e), the V_{22}^d wave-packet component for ^{133}CsI almost reaches the dissociation asymptotic region, whereas the V_{11}^d and V_{22}^d components for ^{135}CsI reach around the left turning point. From this time point the V_{22}^d component for ^{135}CsI heads toward the dissociation asymptote [Figs. 4(f)–4(l)], passing through the AC from the left diabatically around $t =$ 105 232 a.u. (2.55 ps) for the third time, Fig. 4(h), and almost reaching the asymptotic region at $t =$ 135 298 a.u. (3.27 ps), Fig. 4(j). The V_{11}^d component for ^{135}CsI, on the other hand, moves very slowly on V_{11}^d, ascending the slope to the right at $t =$ 105 232 a.u. (2.55 ps), Fig. 4(h), arriving at around the right turning point at $t =$ 135 298 a.u. (3.27 ps), Fig. 4(j), and descending the slope to the left at $t =$ 165 364 a.u. (4 ps). Thus the V_{11}^d component for ^{135}CsI will not go to dissociation in the future.

It seems unusual that the V_{11}^d components already appear at $t =$ 15 033 a.u. (0.36 ps), Fig. 4(b). It is revealed that from the beginning of the temporal propagation very small V_{11}^d components appear around the minimum of V_{11}^d, and then they split into two portions; one remains in the same position throughout the duration of wave-packet propagation as seen in Figs. 4(a)–4(l), and the other moves along with the V_{22}^d component for a while. The V_{11}^d components come from the V_{22}^d counterparts not through the dipole coupling because of no TDM by definition but through the diabatic coupling that has the peak value around the minimum of V_{11}^d as shown in Fig. 1(a). Classical mechanical transition from one state to another is permitted only at the crossing point because of the energy conservation law; it is permitted

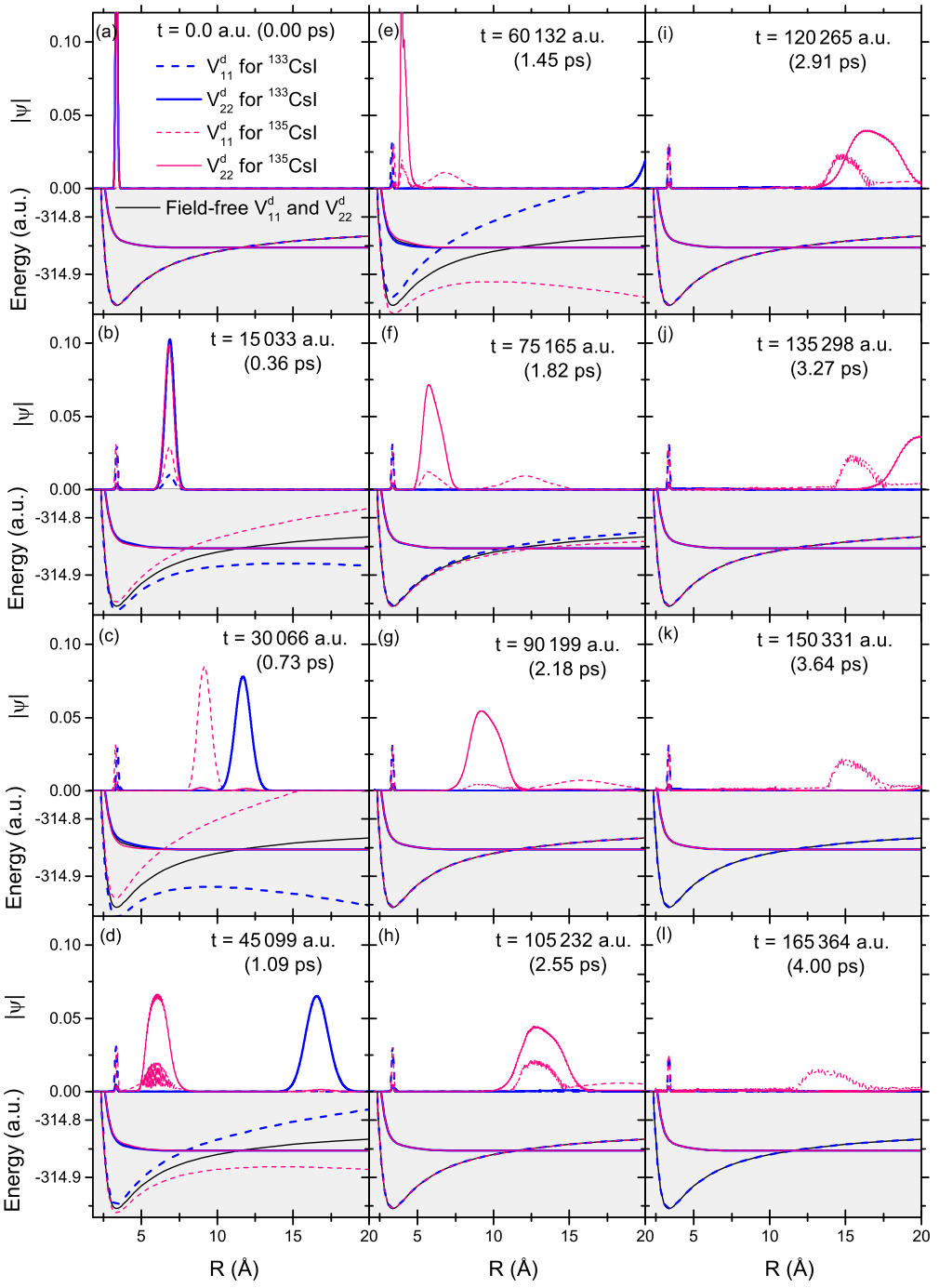

FIG. 4. (Color online) Temporal changes in the V_{11}^d and V_{22}^d wave-packet components (upper panel) along with the temporal shiftings of V_{11}^d and V_{22}^d due to the DSE (lower panel), propagated by the control THz pulse with $T = 82\,682$ a.u. (2 ps) and $E = 5.0\times10^{-3}$ a.u. The wave packets are further propagated under the field-free condition after the field is turned off at $t = 82\,682$ a.u. (2 ps).

quantum mechanically, however, at other points, where the conservation law breaks down.

C. Nonparallel case

One might think of an easier way for isotope-selective dissociation not based on the DSE but on the dependence of electronic transition probability on the field polarization direction relative to the molecular axis [31], which is described as follows. First, using an appropriate laser pulse in the situation where one isotopologue is aligned to a direction and the other is laid in the plane perpendicular to the direction is realized. At this moment, another laser pulse is applied to electronically excite one isotopologue selectively from V_{11}^d to V_{22}^d. Then the excited isotopologue goes down the slope of V_{22}^d toward the dissociation asymptote. Although this scheme is easier, the degree of the alignment directly affects the isotope selectivity. The present temporal wave-packet separation based on the DSE, on the other hand, also needs molecular orientation in the first step but is insensitive to the degree of orientation,

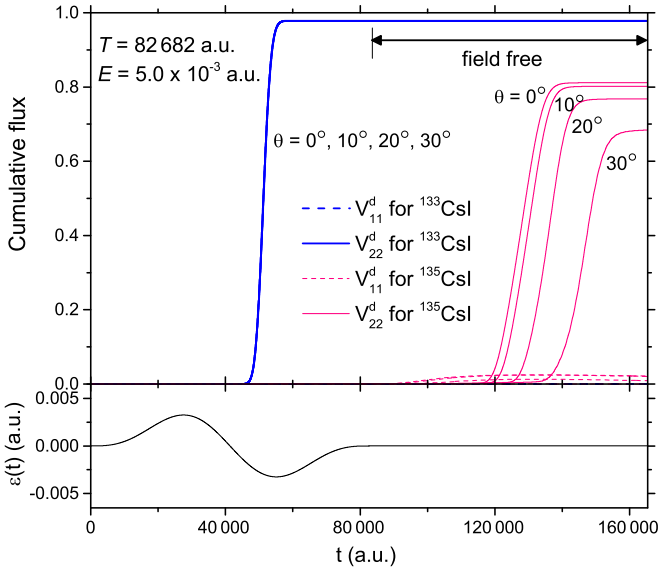

FIG. 5. (Color online) The cumulative fluxes at $R_f = 35$ a.u. for two channels (V_{11}^d and V_{22}^d) of ^{133}CsI and ^{135}CsI, calculated when $T = 82\,682$ a.u. (2 ps), $E = 5.0\times10^{-3}$ a.u., and the angles between the molecular axis and the field polarization direction (θ) are 0°, 10°, 20°, and 30°. The applied THz field is displayed in the lower panel.

which will be numerically demonstrated in this subsection. Considering that the isotope-dependent orientation is not perfectly achieved, we change the angle between the molecular axis and the field polarization direction (θ) and carry out the wave-packet calculations. The THz field with $T = 82\,682$ a.u. (0.5 THz) and $E = 5.0\times10^{-3}$ a.u. is chosen because this combination was found to give the best temporal wave-packet separation for ^{133}CsI and ^{135}CsI [Fig. 3(c)]. The wave packet is propagated for twice as large as T; for the latter half the duration the propagation is performed with the field-free Hamiltonian.

Figure 5 shows the cumulative fluxes at $R_f = 35$ a.u. for two channels (V_{11}^d and V_{22}^d) of ^{133}CsI and ^{135}CsI, calculated for $\theta = 0°$, 10°, 20°, and 30°. The applied THz field is given in the lower panel. As shown in the figure, V_{22}^d cumulative fluxes for ^{133}CsI exhibit a quite similar behavior for all θ's, increasing around $t = 50\,000$ a.u. to nearly 1. In V_{22}^d cumulative fluxes for ^{135}CsI, on the other hand, a difference is seen for different θ's; as θ increases, the rise in the cumulative flux is delayed, and the maximum value is suppressed, which is explained as follows. As θ increases, the upward shifting of V_{11}^d decreases because the interaction between the field and the molecule becomes small. The smaller the upward shifting of V_{11}^d, the smaller the potential energy added to the confined wave packet for ^{135}CsI and the slower the wave-packet movement, and as a result, the later the rise in the cumulative flux. When θ increases, the confined wave packet for ^{135}CsI returning from the right turning point on V_{11}^d tends to pass diabatically through the AC due to the small diabatic coupling, and more portions of the wave packet go down to the well of V_{11}^d, leading, as a result, to a decrease in the maximum of V_{22}^d cumulative flux for ^{135}CsI. Most notable in the figure is that the temporal separation between the V_{22}^d cumulative fluxes for ^{133}CsI and ^{135}CsI is very clear, even when the isotope-dependent orientation is not perfectly achieved; the V_{22}^d cumulative fluxes for ^{133}CsI rapidly rise around $t = 50\,000$ a.u. and those for ^{135}CsI rise around $t = 120\,000 - 150\,000$ a.u.

VII. CONCLUSION

In the present study we have proposed a control scheme of temporal wave-packet separation for oriented molecules based on the nonresonant DSE in the dipole limit. The proposed scheme directly uses the dependence of diabatic coupling on internuclear distance; the transition probability from one diabatic state to another is changed by moving the AC position using the DSE-based potential shifting. As an example of applications of the control scheme, we have considered temporal wave-packet separation for the binary mixture of alkali-halide isotopologues ^{133}CsI and ^{135}CsI using linearly polarized single-cycle THz pulses. We assumed that before applying the control field the perfect isotope-dependent orientation of the isotopologues is achieved and then they are electronically excited from V_{11}^d to V_{22}^d. Calculations of the wave-packet propagation under control THz pulses revealed that the pulse with $T = 82\,682$ a.u. (2 ps) and $E = 5.0\times10^{-3}$ a.u. yielded the best temporal separation of about 2 ps between the ^{133}CsI and the ^{135}CsI photodissociations, among the investigated combinations of T and E. We also considered the cases where the molecular axis is not parallel to the field polarization direction and carried out the same wave-packet calculations. It was found, as a result, that the temporal wave-packet separation for those cases was comparable with that obtained for the perfectly oriented case, suggesting that even when the isotope-dependent orientation is not perfectly achieved, the proposed control scheme based on the nonresonant DSE works well. Since it has been shown that the wave packets of isotopologues can be temporally well separated, the delayed counterpart could be deexcited to the ground-state PEC with another laser pulse, which is possible at least partially with the available laser techniques. It is thus stated that the proposed separation scheme for oriented molecules is more robust against imperfect orientation than the molecular separation technique [33] using the dependence of electronic transition probability on the field polarization direction relative to the molecular axis.

ACKNOWLEDGMENTS

The computations were performed using the supercomputers at the Center for Computational Science & e-Systems, JAEA, Tokai, Ibaraki, Japan and at the Research Center for Computational Science, Okazaki, Aichi, Japan.

[1] S. A. Rice and M. Zhao, *Optical Control of Molecular Dynamics* (Wiley, New York, 2000).

[2] V. S. Letokhov, *Laser Control of Atoms and Molecules* (Oxford University Press, New York, 2007).

[3] M. Shapiro and P. Brumer, *Quantum Control of Molecular Processes* (Wiley-VCH, Weinheim, 2012).
[4] H. Choi, W.-J. Son, S. Shin, B. Y. Chang, and I. R. Sola, J. Chem. Phys. **128**, 104315 (2008).
[5] B. J. Sussman, M. Y. Ivanov, and A. Stolow, Phys. Rev. A **71**, 051401 (2005).
[6] B. J. Sussman, D. Townsend, M. Y. Ivanov, and A. Stolow, Science **314**, 278 (2006).
[7] D. Townsend, B. J. Sussman, and A. Stolow, J. Phys. Chem. A **115**, 357 (2011).
[8] Y.-C. Han, K.-J. Yuan, W.-H. Hu, and S.-L. Cong, J. Chem. Phys. **130**, 044308 (2009).
[9] Y. Liu, Y. Liu, and Q. Gong, Phys. Rev. A **85**, 023406 (2012).
[10] S. Scheit, Y. Arasaki, and K. Takatsuka, J. Phys. Chem. A **116**, 2644 (2012).
[11] S. Scheit, Y. Arasaki, and K. Takatsuka, J. Chem. Phys. **140**, 244115 (2014).
[12] H.-J. Werner and W. Meyer, J. Chem Phys. **74**, 5802 (1981).
[13] A. B. Alekseyev, H.-P. Liebermann, R. J. Buenker, N. Balakrishnan, H. R. Sadeghpour, S. T. Cornett, and M. J. Cavagnero, J. Chem Phys. **113**, 1514 (2000).
[14] Y. Kurosaki, L. Matsuoka, K. Yokoyama, and A. Yokoyama, J. Chem. Phys. **128**, 024301 (2008).
[15] R. Schinke, *Photodissociation Dynamics* (Cambridge University Press, Cambridge, UK, 1993).
[16] H. Sakai, S. Minemoto, H. Nanjo, H. Tanji, and T. Suzuki, Phys. Rev. Lett. **90**, 083001 (2003).
[17] A. Goban, S. Minemoto, and H. Sakai, Phys. Rev. Lett. **101**, 013001 (2008).
[18] O. Ghafur, A. Rouzée, A. Gijsbertsen, W. K. Siu, S. Stolte, and M. J. J. Vrakking, Nat. Phys. **5**, 289 (2009).
[19] L. Holmegaard, J. L. Hansen, L. Kalhøj, S. L. Kragh, H. Stapelfeldt, F. Filsinger, J. Küpper, G. Meijer, D. Dimitrovski, M. Abu-samha, C. P. J. Martiny, and L. B. Madsen, Nat. Phys. **6**, 428 (2010).
[20] S. De, I. Znakovskaya, D. Ray, F. Anis, N. G. Johnson, I. A. Bocharova, M. Magrakvelidze, B. D. Esry, C. L. Cocke, I. V. Litvinyuk, and M. F. Kling, Phys. Rev. Lett. **103**, 153001 (2009).
[21] E. Frumker, C. T. Hebeisen, N. Kajumba, J. B. Bertrand, H. J. Wörner, M. Spanner, D. M. Villeneuve, A. Naumov, and P. B. Corkum, Phys. Rev. Lett. **109**, 113901 (2012).
[22] K. Kitano, N. Ishii, N. Kanda, Y. Matsumoto, T. Kanai, M. Kuwata-Gonokami, and J. Itatani, Phys. Rev. A **88**, 061405 (2013).
[23] R. Honerjäger and R. Tischer, Z. Naturforsch. A **29**, 819 (1974).
[24] G. Audi, A. H. Wapstra, and C. Thibault, Nucl. Phys. A **729**, 337 (2003).
[25] H. Akagi, T. Kasajima, T. Kumada, R. Itakura, A. Yokoyama, H. Hasegawa, and Y. Ohshima, Appl. Phys. B **109**, 75 (2012).
[26] S. Shi and H. Rabitz, J. Chem. Phys. **92**, 364 (1990).
[27] M. D. Feit and J. A. Fleck, Jr., J. Chem. Phys. **78**, 301 (1983).
[28] M. D. Feit and J. A. Fleck, Jr., J. Chem. Phys. **80**, 2578 (1984).
[29] J. Broeckhove, B. Feyen, L. Lathouwers, F. Arickx, and P. Van Leuven, Chem. Phys. Lett. **174**, 504 (1990).
[30] N. Balakrishnan, B. D. Ersy, H. R. Sadeghpour, S. T. Cornett, and M. J. Cavagnero, Phys. Rev. A **60**, 1407 (1999).
[31] C. C. Marston and G. G. Balint-Kurti, J. Chem. Phys. **91**, 3571 (1989).
[32] S. Mahapatra and N. Sathyamurthy, J. Chem. Soc., Faraday Trans. **93**, 773 (1997).
[33] H. Akagi, H. Ohba, K. Yokoyama, A. Yokoyama, K. Egashira, and Y. Fujimura, Appl. Phys. B **95**, 17 (2009).